

V1047 Cen: The first Z And-type outburst observed in the classical nova binary

AUGUSTIN SKOPAL ¹ AND NATALIA SHAGATOVA ¹

¹*Astronomical Institute, Slovak Academy of Sciences,
059 60 Tatranská Lomnica, Slovakia*

ABSTRACT

In 2019, the classical nova V1047 Cen experienced an unusual outburst, the nature of which has not yet been clearly determined. In this paper, we show that the 2019 V1047 Cen outburst is of Z And-type – a type that is characteristic and has so far been observed only in symbiotic binaries. We support our claim by modeling the near-ultraviolet to near-infrared spectral energy distribution, which revealed a close similarity between the fundamental parameters and the mass-loss rate of the burning white dwarf during the 2019 V1047 Cen outburst and those measured during Z And-type outbursts in symbiotic stars. All parameters are in good agreement with the theoretical prediction when the accretion rate exceeds the stable burning limit for white dwarfs with masses $\lesssim 0.7 M_{\odot}$. Our analysis showed that after a nova explosion, the Z And-type outburst can occur not only in symbiotic binaries but also in short-period cataclysmic variables, when the accretion-powered system changes to a nuclear-powered, as a consequence of the donor’s reaction to the nova explosion. Such a development promotes the production of Type Ia supernovae.

Keywords: Cataclysmic variable stars (203) — Classical Novae (251) — Symbiotic binary stars (1674)

1. INTRODUCTION

1.1. Outbursts in accreting white dwarf binaries

Non-magnetic accreting white dwarf binaries in which the white dwarf (WD) accretes from a main-sequence star in Cataclysmic Variables (CVs) or from an evolved giant in Symbiotic Stars (SySts) can produce several types of outbursts (see Warner 1995; Mukai 2017; Balman 2020; Belloni & Schreiber 2023; Sion 2023, for reviews). The response of the WD to mass accretion has been investigated by many authors. It was found that the outcome of accretion and its timescales are basically determined by the accretion rate onto the WD, \dot{M}_{acc} , its mass, M_{WD} , and the WD core temperature (e.g., Paczynski & Zytkow 1978; Sienkiewicz 1980; Nomoto 1982; Yaron et al. 2005; Nomoto et al. 2007; Shen & Bildsten 2007). Accordingly, for this study, we first summarize the main physical phenomena that result from accretion onto a WD of different mass in CVs and/or SySts as follows.

Dwarf novae. When \dot{M}_{acc} is as low as $\lesssim 10^{-10} M_{\odot} \text{ yr}^{-1}$, smaller than the mass transfer rate from the donor, the accretion disk gradually increases its mass up to a critical value at which it becomes hot and luminous due to a viscosity-induced instability, al-

lowing a temporal increase in accretion onto the WD on a timescale of days to weeks. We observe optical brightening in a range of typically 2–6 mag, the so-called dwarf nova (DN) outbursts. These accretion-powered events represent the most frequently observed outbursts in CVs, recurring every few weeks to months, and generating the luminosity of $\approx 10^{34} \text{ erg s}^{-1}$ (e.g., Osaki 1974; Lasota 2001; Mauche 2004; Cannizzo et al. 2012).

Classical novae. Prolonged accretion at a wide range of rates (say, from a few times 10^{-13} to a few times $10^{-7} M_{\odot} \text{ yr}^{-1}$) gradually increases the pressure and temperature of the layer of matter accumulated on the WD surface up to critical values of $\sim 10^{19} \text{ dyn cm}^{-2}$ and $\sim 10^8 \text{ K}$, at which thermonuclear runaway (TNR) is triggered at its base, causing a brightening of the system by up to ~ 15 mag. We observe the so-called classical nova (CN) explosion (e.g., Starrfield et al. 1972; Gallagher & Starrfield 1978; Shara 1989; Bode & Evans 2008; Starrfield et al. 2016). Theoretical modeling of Prialnik & Kovetz (1995) and Yaron et al. (2005) confirmed that the temporal evolution (slow, fast, and recurrent novae, including their extremes), as well as the main properties (e.g., the peak luminosity, the rate of the ejected matter and its expansion velocity) of CNe, can be reproduced

by suitable combinations of three independent parameters: \dot{M}_{acc} , M_{WD} , and the temperature of the WD core.

Accretion onto a low-mass WD ($\lesssim 1 M_{\odot}$) at rather high rates (say, $\gtrsim 10^{-9} M_{\odot} \text{ yr}^{-1}$) produces slow CNe (the time to decline by 2 mag from maximum, $t_2 > 80$ days) with a smaller amplitude ($\lesssim 10$ mag). This is because the bottom of the accreted layer is less degenerate due to less surface gravity, and the temperature may not even reach 10^8 K when (non-explosive) TNR occurs, generating little nucleosynthesis (Fujimoto 1982a,b; Starrfield et al. 2016). Several extreme cases, with a rise to visual maximum over months and a decline to quiescence lasting decades to centuries, were identified as SySts (see Allen 1980), and are therefore called symbiotic novae (SyNe). Following studies showed that TNR can also power SyNe (e.g., Kenyon & Truran 1983), having physical parameters as are typical of CNe in CVs, including the slowest SyN AG Peg (1850 to ~ 1985 , see Kenyon et al. 1993). However, the finding that the total radiation output of SyNe ($10^{46.5} - 10^{47}$ erg) exceeds that of CNe in CVs (see Murset & Nussbaumer 1994) may be the result of efficient mass-transfer via the wind from the evolved giant due to its focusing towards the orbital plane (e.g., Mohamed & Podsiadlowski 2012; Shagatova et al. 2016), which can support the residual burning on the WD surface and thus prolonging the nova lifetime. The latest overview of SyNe was presented by Munari (2024).

In contrast, accretion onto a more massive WD ($> 1 M_{\odot}$) at lower rates (say, $\lesssim 10^{-9} M_{\odot} \text{ yr}^{-1}$) ignites an explosive TNR under degenerate conditions, producing fast CNe ($t_2 < 25$ days) with a higher amplitude ($\gtrsim 10$ mag). If the accretion occurs at a high rate, a few times ($10^{-8} - 10^{-7}$) $M_{\odot} \text{ yr}^{-1}$, the TNR repeats on a timescale of < 100 years. These events are called recurrent (symbiotic) novae (e.g., Yaron et al. 2005).

Supersoft X-ray sources. For specific cases of high \dot{M}_{acc} between a few times 10^{-8} and a few times $10^{-7} M_{\odot} \text{ yr}^{-1}$ and M_{WD} between ~ 0.6 and $\sim 1.35 M_{\odot}$, respectively, hydrogen-rich material can burn stably on the WD surface, i.e., at the same rate as it is accreted (see e.g., Fig. 1 of Wolf et al. 2013). The corresponding nuclear energy output, typically of $10^{36} - 10^{38} \text{ erg s}^{-1}$, is emitted in the supersoft X-ray energies below ~ 1 keV. Therefore, these objects are called supersoft X-ray sources (SSSs, e.g., van den Heuvel et al. 1992; Greiner 1996a). Due to extreme absorption in this domain, not all stable burning WDs can be observed as SSSs. This is the case for many nuclear-powered SySts, of which only a few are reliably observed as SSSs. For example, symbiotic X-ray binaries, AG Dra ($N_{\text{H}} = 3.15 \times 10^{20} \text{ cm}^{-2}$, González-Riestra et al. 2008), LIN 358 ($N_{\text{H}} = 6.1 \times 10^{20} \text{ cm}^{-2}$, Skopal 2015), and Draco C1 ($N_{\text{H}} = 4.3 \times 10^{20} \text{ cm}^{-2}$,

Saeedi et al. 2018). Basically, we observe persistent SSSs (see a catalog of Greiner 1996b) or transient (recurrent) sources, such as the SSS phase of CNe.

Z And-type outbursts. When \dot{M}_{acc} exceeds the level sustaining stable burning ($\gtrsim 10^{-7}$) $M_{\odot} \text{ yr}^{-1}$, the material will still burn stably (i.e., generate the luminosity of a few times $10^{37} \text{ erg s}^{-1}$), but not at the same rate as it is accreting. The burning cannot consume all the accreted material, which leads to the formation of a red-giant-like structure (e.g., Paczynski & Rudak 1980; Nomoto 1982) or the blowing of an optically thick wind from the WD at rates $\gtrsim 10^{-6} M_{\odot} \text{ yr}^{-1}$ (e.g. Kato & Hachisu 1994; Hachisu et al. 1996)¹. These events are observationally indicated by a few magnitudes brightening in the optical, evolving on a timescale of weeks to years (e.g., Belyakina 1991; Skopal 2008; Leibowitz & Formiggini 2008; Sekeráš et al. 2019), always accompanied by an enhanced mass outflow (e.g., Fernandez-Castro et al. 1995; McKeever et al. 2011) at rates of a few times $10^{-6} M_{\odot} \text{ yr}^{-1}$, and terminal velocities of $(1 - 3) \times 10^3 \text{ km s}^{-1}$ (Skopal 2006; Sonith & Kamath 2023). They are called Z And (-type) outbursts because they were observed in the past for the prototype of the class of SySts – Z And (see Fig. 1.2 of Kenyon 1986). So far, they have been observed exclusively in the light curves of SySts. It was found that during Z And-type outbursts the luminosity of the burning WD, L_{WD} , is several times $10^{37} \text{ erg s}^{-1}$, its effective radius, $R_{\text{WD}}^{\text{eff}}$, is around $0.1 R_{\odot}$, the blackbody temperature, T_{WD} , is $(1 - 2) \times 10^5$ K, and the emission measure of the nebular continuum, EM , is a few times 10^{60} cm^{-3} (Mueret et al. 1991; Skopal 2005; Kato et al. 2012; Skopal et al. 2017; Cúneo et al. 2018). The nebular emission represents a part of the hot WD radiation converted by the fast wind flowing from the WD at rates, $\dot{M}_{\text{WD}} \gtrsim 10^{-6} M_{\odot} \text{ yr}^{-1}$ (Seaquist & Taylor 1992; Skopal 2006; Skopal et al. 2017, 2020). Both the L_{WD} and \dot{M}_{WD} derived from observations are consistent with the theoretical prediction mentioned at the beginning of this paragraph.

Finally, we note that the post-outburst evolution of CN may be affected by a significant increase in mass transfer due to irradiation of the donor by the nova explosion (Kovetz et al. 1988; Hillman et al. 2020; Ginzburg & Quataert 2021). This effect can explain

¹ The principle of Z And-type outbursts was already postulated by Tutukov & Yungelson (1976). However, the lack of knowledge of the accurate WD’s parameters during these outbursts (luminosity and mass-loss rate) meant that their true nature was not clear for a long time (see Sect. 4.3.2 of Mueret et al. (1991), Sect. 3.3 of Tomov et al. (2016), and Sect. 4.2 of Skopal et al. (2017)).

the transition from an accretion-powered system before the SyN outburst to a nuclear-powered system after it, which may subsequently lead to the triggering of a Z And-type outburst (see Sect. 4.9 of Skopal et al. 2017). In the case of some CNe (e.g., GQ Mus and V723 Cas, Oegelman et al. 1993; Ness et al. 2008) and very luminous SSSs, this effect may support residual surface nuclear burning, which helps to understand their unusually long-lasting and luminous SSS phases (see Skopal 2022).

Here, in the case of the CN V1047 Cen, we show that its unusual 2019 outburst is analogous to the Z And-type outburst in SySts that occur after their SyN outburst (see Fig. 12 of Skopal et al. 2020).

1.2. Classical nova V1047 Cen and its 2019 outburst

The explosion of the CN V1047 Cen (Nova Cen 2005) was discovered by Liller et al. (2005) on 2005 September 1.03 at a visual magnitude of 8.5. The authors supported the nature of the transient as a CN with a spectrum obtained a few days later. Subsequent spectroscopic observations specified the ‘Fe II’ type of this nova (Walter et al. 2012). According to Aydi et al. (2022), the progenitor’s brightness of $V > 20.5 - 21$ corresponds to the nova amplitude of $\Delta V \approx 13$ mag and an absolute magnitude of $M_V > 5$, both of which favor a typical cataclysmic variable containing a main-sequence donor star.

Another outburst of V1047 Cen was recorded on 2019 June 11 by Delgado et al. (2019) as a transient AT2019hik/Gaia19cfn. Based on the Optical Gravitational Lensing Experiment survey (OGLE; Udalski et al. 2015), Mroz & Udalski (2019) unambiguously associated the transient with V1047 Cen and found that the re-brightening started already on 2019 April 6.11 with a gradual increase by ~ 2.5 mag measured on 2019 June 12.04 in the OGLE I band. The authors noted that such slow brightening is not consistent with a recurrent nova explosion.

This unexpected outburst led to subsequent spectroscopic monitoring of V1047 Cen in the optical and near-infrared (NIR) (see Aydi et al. 2019a,b; Di Mille et al. 2019; Geballe et al. 2019a), while the BVR_{CI} photometry was performed by amateur astronomers and collected in the AAVSO database. Analyzing NIR spectroscopy, broadband optical, and NIR photometry during the first 160 days of the 2019 outburst, Geballe et al. (2019b) concluded that the outburst is most likely a dwarf nova eruption. However, the authors discussed its long duration and too-early appearance after the CN outburst as the main shortcomings of this interpretation. Based on multiwavelengths, near-ultraviolet to radio, observations spanning the entire, more than 400-day

lasting outburst, Aydi et al. (2022) suggested “that the outburst may have started with a brightening of the disk due to enhanced mass transfer or disk instability, possibly leading to enhanced nuclear shell burning on the white dwarf, which was already experiencing some level of quasi-steady shell burning.” The authors pointed to observational similarities with outbursts in SySts. The exceptionality of this outburst led the authors to conclude that “the 2019 outburst of V1047 Cen appears to be unique, and nothing similar has been observed in a typical cataclysmic variable system before, hinting at a potentially new astrophysical phenomenon.”

Here, analyzing the observations of Geballe et al. (2019b) and Aydi et al. (2022) using the method of multiwavelength modeling of the spectral energy distribution (SED) in the composite spectra of SySts (see Skopal 2005), we classify the 2019 V1047 Cen outburst as a Z And-type, commonly produced by WDs in SySts. To achieve our goal, we show that the fundamental parameters of the burning WD (L_{WD} , R_{WD}^{eff} , T_{WD}) and its \dot{M}_{WD} during the 2019 V1047 Cen outburst, are comparable to those of the Z And-type outbursts, and the pre- and post-outburst luminosities are consistent with stable hydrogen burning on the WD surface.

Accordingly, in Sect. 2 we describe and present the results of our analysis, while a discussion and conclusion are found in Sects. 3 and 4, respectively.

2. ANALYZIS AND RESULTS

2.1. Selection of days for SED modeling

Based on observations covering the 2019 outburst of V1047 Cen (see Geballe et al. 2019b; Aydi et al. 2022), we modeled the SED from the near-ultraviolet (NUV) to the NIR, from 0.1928 to 4.60 μm . We used *Swift*-UVOT $UVW2$, $UVM2$, optical BVR_{CI} , NIR JHK and NEOWISE $W1$, $W2$ photometry complemented with optical ($\sim 0.4 - 0.9 \mu\text{m}$) and NIR (0.9 – 2.5 μm) spectroscopy.

Before the outburst maximum (see Fig. 2 a, dotted vertical line), we reconstructed the observed SED for days 86 and 118², when the absolute fluxes of simultaneous NIR photometry and NIR spectroscopy were available and in good agreement. The corresponding UVOT magnitudes were estimated by interpolating the closest observations to these days. During the maximum brightness (days 264 to 331), we selected day 308 because of the simultaneous NUV and $W1$, $W2$ NIR photometry were available. Finally, after the outburst, we reconstructed the model SED using the $UVW2$ mag-

² Days since the outburst onset, 2019 April 6.11 (see Sect 1.2).

Table 1. Physical Parameters of the 2019 Outburst of the Nova V1047 Cen Determined by SED Modeling^a.

Age ^b (JD-JD ₀)	T_e (kK)	EM (10^{60} cm^{-3})	T_{WD} (kK)	$R_{\text{WD}}^{\text{eff}}$ (R_{\odot})	L_{WD} ($10^{37} \text{ erg s}^{-1}$)	\dot{M}_{WD} ($10^{-6} M_{\odot} \text{ yr}^{-1}$)
86	30±5	1.4±0.1	175±10 ^c	0.13±0.01	5.50±0.80	1.34±0.11
118	30±5	3.3±0.2	176±10 ^c	0.13±0.01	5.45±0.90	2.05±0.15
308	20±3	4.9±0.3	136±10 ^c	0.20±0.02	4.91±0.90	3.16±0.27
407	40±5	0.13±0.02	~190	~0.07	~2	~0.28

Notes.^a Designation as in Sections 2.2 and 2.3,^b JD₀ = 2 458 579.61 (2019 April 6.11) is the date of the outburst beginning.^c Interpolated values from Table 3 to dates of the SED models (full circles in Fig. 2 d).

nitude (day 413), emission-line-free optical magnitudes (days 402 to 436) and $W1$, $W2$ fluxes (day 469).

Optical and NIR magnitudes were converted to fluxes according to the calibration of Henden & Kaitchuck (1982), while the NUV magnitudes were calibrated using the UVOT photometric system (see Poole et al. 2008). To obtain photometric flux points of the true continuum, we determined corrections for emission lines from the used spectra (see Appendix A, Table 2). The emission-line-free BVR_CI_C photometry was used to verify the flux calibration of the optical spectra and for the color-diagram diagnostic in Sect. 2.4. In all cases, observations obtained not simultaneously with the selected day were calibrated using optical magnitudes corrected for emission lines. This is justified by the dominance of the nebular continuum in the optical/NIR (see Sect. 2.2).

Observations were dereddened with $E_{B-V} = 1.0$ and the distance-dependent parameters were scaled to a distance of 3.2 kpc (Aydi et al. 2022).

2.2. SED modeling and corresponding parameters

In modeling the NUV to NIR continuum we assumed that the measured spectrum, $F(\lambda)$, consists of the stellar component of radiation from the hot WD pseudophotosphere, and the nebular continuum emitted by the hydrogen plasma. The presence of these components of radiation in the spectrum is supported by the presence of emission lines of ions with a high ionization potential (e.g., C IV, He II, H I, see Aydi et al. 2022). Because of a high T_{WD} , we observe only the long-wavelength tail of the WD’s radiation in the NUV/optical, which can be approximated by a blackbody radiation. Thus, the reddening-free continuum of V1047 Cen measured at the Earth, can be written in the form (see Skopal et al. 2017)

$$F(\lambda) = \theta_{\text{WD}}^2 \pi B_{\lambda}(T_{\text{WD}}) + k_{\text{N}} \varepsilon_{\lambda}(\text{H}, T_e), \quad (1)$$

where the angular radius of the WD pseudophotosphere θ_{WD} ($= R_{\text{WD}}^{\text{eff}}/d$) scales the blackbody flux to the spec-

trum, and it is given by its effective radius $R_{\text{WD}}^{\text{eff}}$ and the distance d . The observed emission measure, k_{N} (cm^{-5}), scales the volume emission coefficient $\varepsilon_{\lambda}(\text{H}, T_e)$ ($\text{erg cm}^3 \text{ s}^{-1} \text{ \AA}^{-1}$) of the nebular continuum to observations: $k_{\text{N}} = EM/4\pi d^2$ (Skopal 2005) and $EM = \int_V n_e n_p dV$ is the emission measure of the hydrogen nebula given by the electron and proton concentrations, n_e and n_p , in the volume V . The parameter T_e is the electron temperature.

To model the measured SED by Eq. (1), we first estimated the parameters k_{N} and T_e from the grid of models (1), which determine the amount and the slope of the nebular continuum, respectively. Second, we added a blackbody radiation for independently determined T_{WD} (see below) to fit the NUV fluxes as well. In this way we estimated the fitting parameters θ_{WD} , T_e , and k_{N} . Consequently, $R_{\text{WD}}^{\text{eff}} = d\theta_{\text{WD}}$, $EM = 4\pi d^2 k_{\text{N}}$, and $L_{\text{WD}} = 4\pi d^2 \theta_{\text{WD}}^2 T_{\text{WD}}^4$. The SED models are depicted in Fig. 1, resulting parameters are listed in Table 1 and their temporal evolution is shown in Fig. 2.

We estimated the temperature T_{WD} from the He II $\lambda 4686/\text{H}\beta$ flux ratio (e.g., Gurzadyan 1997). Here, we used the approach of Skopal et al. (2020), who calculated this ratio for $T_e = 30,000$ and $20,000$ K, which suits our models (Table 1). To determine the flux ratio of these lines, we scaled the spectra to the emission coefficient $\varepsilon_{\lambda}(\text{H}, T_e)$ because the nebular continuum dominates the optical/NIR (see Fig. 1). The method is valid for T_{WD} between 70,000 and 200,000 K (Iijima 1981). Table 3 lists values of T_{WD} for spectra of Aydi et al. (2022) that contain satisfactorily exposed He II $\lambda 4686$ and H β emission lines. More details and error estimation are given in Appendix C.

Due to the dominance of the nebular continuum in the optical/NIR, Eq. (1) reduces to, $F(\lambda) = k_{\text{N}} \varepsilon_{\lambda}(\text{H}, T_e)$, which allows us determining the parameter k_{N} for any known flux-point in this domain. For example, the flux

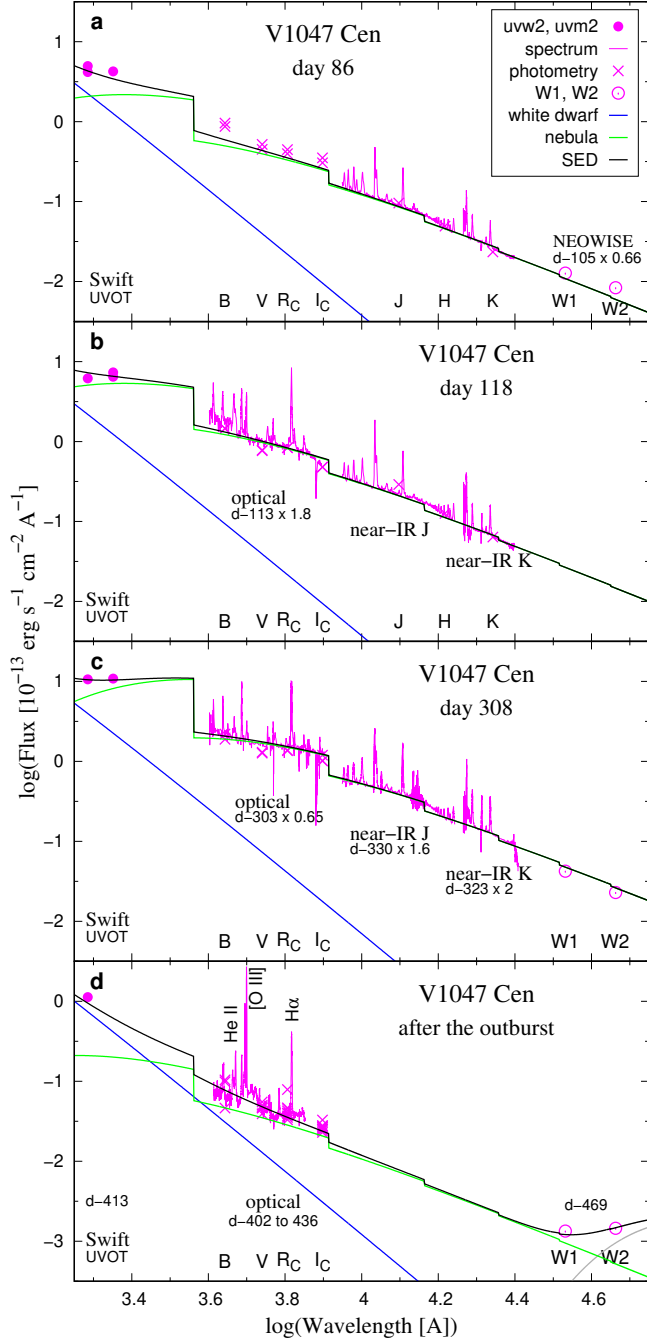


Figure 1. The observed (in magenta) and modeled (black line) SEDs of V1047 Cen at selected days (Sect. 2.1) during its 2019 outburst (panels **a**, **b**, and **c**) and after it (**d**). The meaning of the lines and symbols is shown in the keys. After the outburst, the NIR W1, W2 fluxes are affected by a third light, interpreted by Aydi et al. (2022) as a ~ 400 K warm dust emission. Modeling is described in Sect. 2.2.

$F(V)$ of the emission-line-free V magnitude determines the emission measure as

$$EM = 4\pi d^2 \frac{F(V)}{\varepsilon_V(H, T_e)}, \quad (2)$$

where we used $\varepsilon_V(H, 30,000 \text{ K}) = 3.6$ and $\varepsilon_V(H, 20,000 \text{ K}) = 4.2 \times 10^{-29} \text{ erg cm}^3 \text{ s}^{-1} \text{ \AA}^{-1}$ before and after day 264, respectively (see Fig. 3a). Having EM and T_{WD} we can determine L_{WD} and thus $R_{\text{WD}}^{\text{eff}}$ under the assumption that all the ionizing photons produced by the hot WD pseudophotosphere are converted to nebular emission (see Appendix B in detail). These parameters are introduced in Table 3 and shown in Fig. 2 as open circles. However, after the outburst (day 407), this approach is not applicable because the flux of ionizing photons exceeds the rate of recombinations required by the measured EM by a factor of >20 . The uncertainties of all parameters are described in Appendix C.

2.3. Mass-loss rate from the WD

Modeling the broad $H\alpha$ wings, which develop during Z And-type outbursts of SySts, Skopal (2006) showed that they are emitted by a fast ionized wind flowing from the hot WD at rates, \dot{M}_{WD} , of a few times ($10^{-7} - 10^{-6}$) $M_{\odot} \text{ yr}^{-1}$. Furthermore, the finding that the EM of broad $H\alpha$ wings is comparable to that of symbiotic nebulae implies that the nebular emission in active SySts can be attributed to the emission of the ionized wind from their hot components (see Sect. 4.2. there). Since the emission lines as well as the nebular continuum arise in the same ionized volume, the value of \dot{M}_{WD} can be determined from the EM and the given wind model. Here, we used the relationship between EM and \dot{M}_{WD} derived by Skopal et al. (2017) for a spherically symmetric, β -law wind of Lamers & Cassinelli (1999),

$$EM = \xi \left(\frac{\dot{M}_{\text{WD}}}{v_{\infty}} \right)^2 \frac{1}{bR_0(1-2\beta)} \left[1 - \left(1 - \frac{bR_0}{R_{\text{in}}} \right)^{1-2\beta} \right]. \quad (3)$$

The wind starts at the radial distance $r = R_0$ from the WD centre with the initial velocity a and becomes optically thin at $r = R_{\text{in}} \equiv R_{\text{WD}}^{\text{eff}}$. The wind velocity profile is characterized by the acceleration factor β and the terminal velocity v_{∞} . The parameter $\xi = 1.45 \times 10^{46} \text{ g}^{-2}$ and $b = 1 - (a/v_{\infty})^{1/\beta}$. We determined \dot{M}_{WD} for EM in Tables 1 and 3, $v_{\infty} = 1700 \text{ km s}^{-1}$ (Aydi et al. 2022), $\beta = 1.7$ and $a = 50 \text{ km s}^{-1}$ (Skopal et al. 2017). For the value of R_0 , we considered two limiting cases: $R_0 = R_{\text{WD}}^{\text{eff}}$ and $R_0 = R_{\text{WD}} (\equiv 0.01 R_{\odot})$, which correspond to the lower and upper limits of \dot{M}_{WD} , respectively. The averages of these limiting \dot{M}_{WD} are given in Tables 1 and 3 and shown in Fig. 2e. Their uncertainties are described in Appendix C.

2.4. Color-diagram diagnostics

Here, using the multicolor photometric observations, we independently support the main result of the SED

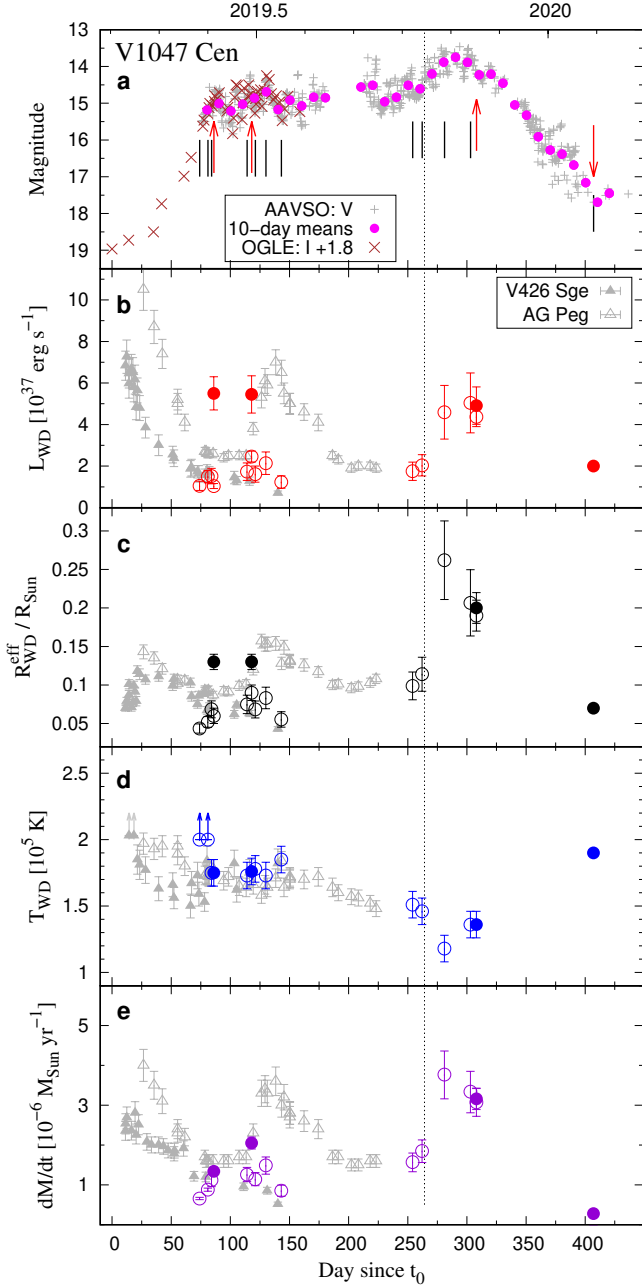


Figure 2. Evolution of the V/I light curve (panel **a**), and parameters L_{WD} (**b**), $R_{\text{WD}}^{\text{eff}}$ (**c**), T_{WD} (**d**), and \dot{M}_{WD} (**e**) throughout the 2019 outburst of V1047 Cen. The full circles in panels **b** to **e** are from Table 1, while the open circles are from Table 3. Vertical bars in panel **a** denote the acquisition dates of the spectra used to determine T_{WD} (Table 3), while the red arrows indicate the dates of the SED models (Table 1). The vertical dotted line (day 264) indicates the time just before the main brightening. The gray triangles are for comparison with the values determined during Z And-type outbursts of SySts AG Peg and V426 Sge (data from Skopal et al. 2017, 2020).

modeling – the presence of a strong nebular continuum that dominates the optical/NIR during the 2019 outburst of V1047 Cen.

For this purpose, we reconstructed the reddening-free and line-free $V - I_C/\text{time}$, and $B - V/V - I_C$ diagrams and compared them with the corresponding theoretical diagrams calculated for hydrogen nebular continuum emitting at different T_e . The result is shown in Fig. 3, the reconstruction of which is described in Appendix D.

From the first observations on day 77 to day ~ 264 (green points), the $V - I_C$ index shows a plateau phase with values scattered around 0.76 mag that corresponds to $T_e \sim 30,000$ K. Relatively stable T_e also implies a relatively stable temperature of the ionization source T_{WD} – in good agreement with SED models from this period (days 86 and 118, Table 1). During the following period, from day ~ 264 to day ~ 331 (red points), when the outburst reached its optical maximum, the $V - I_C$ index has increased to ~ 1.05 mag, which corresponds to $T_e \sim 15,000$ K and suggests a decrease in T_{WD} – also consistent with the SED model performed just after the maximum brightness (day 308, Table 1). During the decline of the outburst, from day ~ 343 to day ~ 402 (violet points), the $V - I_C$ and $B - V$ indices were significantly affected by the appearance of a strong nebular $[\text{O III}] \lambda 5007$ line in the spectrum (Aydi et al. 2022), which is located at the steep short-wavelength edge of the V filter, and thus can cause a large scatter in the photometric measurements obtained by different instruments (see Fig. 8 of Chochol et al. 1993). The $B - V/V - I_C$ diagram (panel **b**) confirms the properties of the nebular continuum suggested by the behavior of the $V - I_C$ index.

A comparison of the observed and theoretical color indices confirms the dominant presence of the nebular continuum in the spectrum and changes in its T_e as revealed by SED modeling.

2.5. The WD luminosity outside the 2019 outburst

Based on the brightness excess between the 2005 and 2019 outbursts (the average OGLE $I = 17.1$ and $V = 17.5$ mag between 2013 and 2019) compared to the pre-nova outburst ($V \gtrsim 20.5 - 21$) and the blue reddening-free $V - I$ index, Aydi et al. (2022) concluded that the luminosity of the WD before the 2019 outburst was powered by a stable nuclear burning on its surface. After the 2019 outburst, the authors supported this scenario by the presence of high ionization lines in the late spectrum of V1047 Cen (days 407, 615, 643, and 774), which is a signature of the nuclear burning in a shell on the WD surface (e.g. Sokoloski et al. 2016) and the presence of collimated outflow during this period that is also

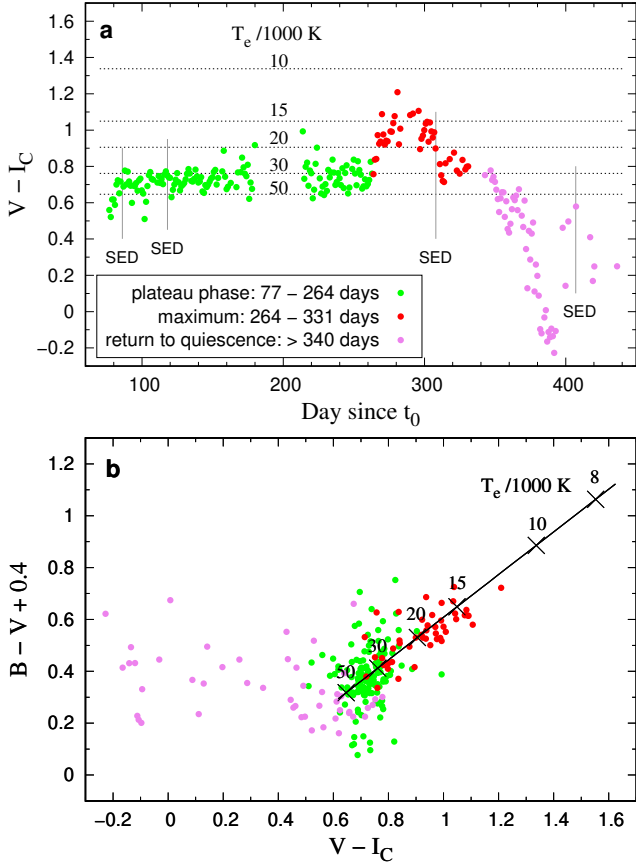


Figure 3. Color-diagram diagnostics of the 2019 outburst of V1047 Cen. The panel **a** shows the evolution of the $V - I_C$ color index along the outburst, while the panel **b** shows the $B - V / V - I_C$ color diagram. Dotted lines in panel **a** and the solid line in panel **b** correspond to the theoretical values of the hydrogen nebular continuum calculated for different electron temperatures T_e , marked by labels. Different colors distinguish specific parts of the light curve as indicated in the keys. The good agreement between the measured and theoretical values confirms the dominant contribution of the nebular continuum in the optical spectrum, as found by SED modeling (see Fig. 1, Sect. 2.4).

sometimes observed in the spectra of SySts at/after their major Z And-type outbursts (e.g., Z And, BF Cyg, see Skopal et al. 2009, 2013).

Here, we support this suggestion with a model SED from the 2019 post-outburst period (Fig. 1 d), when the brightness of V1047 Cen dropped to its pre-outburst value, $V \sim 17.5$ mag. The model shows that the decrease in brightness by ~ 4 mag in the optical during 100 days after the maximum was mainly due to the decrease in EM by a factor of ~ 40 , which corresponds to a decrease in the mass-loss rate by a factor of $\gtrsim 10$, $\dot{M}_{\text{WD}} \sim 2.8 \times 10^{-7} M_{\odot} \text{ yr}^{-1}$. As a result, the optically

thick/thin wind interface has shrunk to $R_{\text{WD}}^{\text{eff}} \sim 0.07 R_{\odot}$, while the increased $\text{He II } \lambda 4686$ emission ($\approx F(\text{H}\beta)$) indicated a high T_{WD} of ~ 190 kK, which corresponds to a still high L_{WD} of $\sim 2 \times 10^{37} \text{ erg s}^{-1}$ (see Table 1). This value is well explained by the nuclear burning of hydrogen-rich material on the surface of the WD at a rate of $\sim 7.2 \times 10^{-8} M_{\odot} \text{ yr}^{-1}$ ³ driven by accretion from the donor and remnant mass from the 2019 outburst.

3. DISCUSSION

3.1. Classification of the 2019 V1047 Cen outburst

The values of the WD parameters and the wind-mass-loss rate during the 2019 V1047 Cen outburst (Table 1, Fig. 2), and its pre- and post-outburst luminosities, which are consistent with stable hydrogen burning on the surface of the WD (see Sect. 2.5), allow the 2019 outburst to be classified as of the Z And-type, commonly observed in SySts (see Sect. 1.1).

The key to this interpretation is the emergence of strong nebular emission in the spectrum during the outburst (see Figs. 1 and 3). Its high value, characterized by $EM \gtrsim 10^{60} \text{ cm}^{-3}$, requires a strong ionization source in the system producing $\gtrsim 10^{47}$ hydrogen ionizing photons per second, which at the temperature of $\sim 1.6 \times 10^5 \text{ K}$ corresponds to the luminosity of $\gtrsim 10^{37} \text{ erg s}^{-1}$ (see Table 3). Such a strong ionization source is represented by a nuclear-burning WD in V1047 Cen.

According to the SED models, the WD average luminosity of $5.3 \times 10^{37} \text{ erg s}^{-1}$ (see the 6th column in Table 1) requires $\dot{M}_{\text{acc}} \sim 2 \times 10^{-7} M_{\odot} \text{ yr}^{-1}$ throughout the 2019 outburst⁴, which is above the upper limit of stable burning for a WD mass $\lesssim 0.7 M_{\odot}$ (see e.g., Fig. 1 of Wolf et al. 2013). Since the nebular emission represents a fraction of the WD radiation converted by wind particles, its marked increase during the outburst reflects a corresponding increase in the \dot{M}_{WD} (Sect. 2.3). In our case, $EM \gtrsim 10^{60} \text{ cm}^{-3}$ corresponds to $\dot{M}_{\text{WD}} \gtrsim 10^{-6} M_{\odot} \text{ yr}^{-1}$ throughout the 2019 outburst – the value proposed by theory when the accretion rate on a WD increases above the level sustaining stable burning (see Sect. 1.1).

Therefore, according to the values of the L_{WD} and \dot{M}_{WD} parameters, the 2019 V1047 Cen outburst can be classified as a Z And-type.

3.2. The origin of the brightness variability

³ $\dot{M}_{\text{acc}} = L_{\text{WD}} / \eta / X$, where $\eta = 6.3 \times 10^{18} \text{ erg g}^{-1}$ is the hydrogen-burning energy production from 1 gram, and $X \equiv 0.7$ is the hydrogen mass fraction in the accreted matter.

⁴ i.e., during the main part of the outburst covered by multiwavelength observations, from day ~ 74 to day ~ 340 .

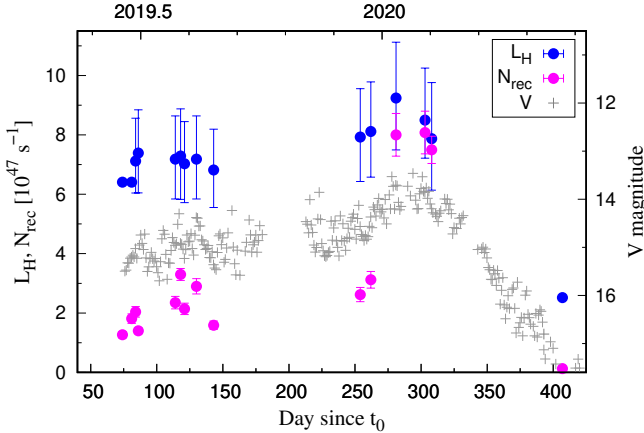


Figure 4. Evolution of the flux of hydrogen-ionizing photons, L_H , generated by the hot WD pseudophotosphere, and the rate of recombinations, N_{rec} , in the ionized wind along the 2019 V1047 Cen outburst (Appendix B). The 1-day means of V magnitude are compared. The variations in N_{rec} reflect those in EM , \dot{M}_{WD} , and hence the observed brightness variations (Sect. 3.3).

Due to the dominance of the nebular continuum in the optical/NIR (Fig. 1), an increase in brightness corresponds to a higher EM (Eq. (2)), and thus a higher \dot{M}_{WD} (Eq. (3)), and vice versa. Accordingly, variations in the optical light curve on a timescale of several days to tens of days, with an amplitude of $\lesssim 1$ mag, observed along the 2019 outburst (Aydi et al. 2022, Fig. 2 a here) as well as the main brightening after day ~ 264 , can be explained by the variable wind from the burning WD.

The connection between the star’s brightness and \dot{M}_{WD} is also supported by the broad emission wings of the H I and He I lines ($\sim 2,000 \text{ km s}^{-1}$) with variable P Cyg type absorption components at the beginning of the first flat-peak phase of the outburst (see Fig. 3 of Geballe et al. 2019b), and during the maximum (day $\gtrsim 264$), when the enhanced \dot{M}_{WD} (see Fig. 2e) was evidenced by the reappearance of strong P Cygni profiles in the line spectrum (see Aydi et al. 2022).

Therefore, it is natural to assume that the observed variability is caused by variable mass transfer from the donor during the outburst, which means a variable accretion that is still above the stable burning limit ($\dot{M}_{\text{WD}} \gtrsim 10^{-6} M_{\odot} \text{ yr}^{-1}$) and hence a variable mass-loss rate causing the observed brightness variability.

3.3. The WD luminosity during the 2019 outburst

The determination of L_{WD} from SED models (day 86, 118 and 308) is given by the temperature, T_{WD} , and scaling, θ_{WD} , of the WD radiation to the observed NUV to NIR SED (Sect. 2.2). Despite the significantly different

T_{WD} (Table 3) and θ_{WD} between the first part of the outburst (days 86 and 118) and around the maximum (day 308), the corresponding L_{WD} is stable (within the uncertainties), with an average value of $5.3 \times 10^{37} \text{ erg s}^{-1}$, throughout the outburst (Table 1, Fig. 2 b).

The estimate of L_{WD} from the nebular continuum assumes an equilibrium between the flux of hydrogen-ionizing photons, L_H , generated by the hot WD pseudophotosphere and the rate of recombinations, N_{rec} , in the wind (see Appendix B). Figure 4 shows that values of L_H are comparable (within the uncertainties) during the outburst, while values of N_{rec} correlate with the star’s brightness. The former is a result of a constant L_{WD} at high T_{WD} (see Eq. (B3), while the latter is given by variations in the EM (according to Eqs. (B4) and (2), $V = \log(N_{\text{rec}}) + \text{const.}$).

During the first part of the 2019 outburst (days < 264), $L_H > N_{\text{rec}}$. This means that a fraction of ionizing photons escapes the nebula without being converted to nebular radiation. In other words, the wind particles are unable to convert all ionizing photons into nebular radiation. As a result, the corresponding EM provides values of L_{WD} according to Eq. (B1) (open circles in Fig. 2 b), which are smaller than the true values (full circles in the figure).

During the maximum, $L_H \sim N_{\text{rec}}$, which means that all ionizing photons are absorbed by the wind particles and converted into nebular radiation – we measure a maximum EM in the spectrum for a given L_H . As a result, L_{WD} obtained from both, EM (Eq. (B1) and SED models are comparable (see Fig. 2 b).

3.4. Consistency with the optically thick wind theory

The nature of the 2019 outburst of the Nova V1047 Cen also dictates the mutual consistency of the WD parameters, L_{WD} , $R_{\text{WD}}^{\text{eff}}$, T_{WD} , \dot{M}_{WD} , and T_e of the ionized wind: A higher \dot{M}_{WD} creates a larger optically thick/thin wind interface above the WD surface (i.e., a larger $R_{\text{WD}}^{\text{eff}}$) resulting in a lower T_{WD} that is responsible for a lower T_e , and vice versa. The parameters we obtained during the first flat-peak phase of the outburst and during its maximum well express this relationship (see Fig. 2, Sect. 2.4). This is consistent with the theory of the optically thick wind in outbursts on the WD surface (see Kato & Hachisu 1994).

3.5. Comparison with Aydi et al. (2022)

Although DN outbursts occasionally occur in CN binaries, observations of the 2019 outburst in the CN V1047 Cen were controversial in this regard (see Geballe et al. 2019b). Also, Aydi et al. (2022) questioned the possibility of a DN at the beginning of the 2019 outburst due to the high accretion rate and heating of the

accretion disk during the stable burning phase between the 2005 and 2019 outbursts. Based on the multiwavelength observations, Aydi et al. (2022) came to a conclusion that this event may have started with a brightening of the disk, which then triggered enhanced nuclear shell burning on the WD surface. The authors also pointed out that the 2019 outburst had many observational similarities to outbursts of classical SySts. However, without deriving correct parameters (compare their SED model in Fig. 14 and our one in Fig. 1 here), the authors were unable to clearly classify the outburst, even admitting the possibility of a *”record breaking dwarf nova outburst or a new phenomenon”*.

Our classification of the 2019 V1047 Cen outburst as a Z And-type is given by the following results:

- Before and after the outburst, L_{WD} corresponded to values generated by a stable-burning WD (see Sect. 2.5).
- During the outburst (from day ~ 74 to ~ 340), the high $L_{\text{WD}} \sim 5.3 \times 10^{37} \text{ erg s}^{-1}$ requires fueling at $\dot{M}_{\text{acc}} \sim 2 \times 10^{-7} M_{\odot} \text{ yr}^{-1}$ that is above the stable burning limit for a WD mass $\lesssim 0.7 M_{\odot}$.
- At the same time, $\dot{M}_{\text{WD}} \gtrsim 10^{-6} M_{\odot} \text{ yr}^{-1}$ was indicated (see Sect. 3.1).

These properties constitute the basic conditions for classifying the outburst as a Z And-type (see Sect. 1.1).

In agreement with the above-mentioned papers, there is no reason for the appearance of a DN outburst during this main part of the 2019 outburst. Also, the gradual brightening during the first two months after the outburst onset suggests a gradual increase in the accretion throughout the disk, and not a one-time brightening due to disk instability since the profile of the ascending part of the 2019 outburst does not match that of a DN outburst. Accordingly, it is possible to imagine that a gradual increase in the mass transferred through the disk, will cause the disk, and consequently, the WD, gradually brightens. Since the nuclear hydrogen burning is a factor of ~ 50 more efficient than the release of radiation by the accretion process, it is possible to conclude that the initial brightening by $\gtrsim 4 \text{ mag}$ is the result of the gradual feeding of a stable burning WD to the upper limit, at/above which the unconsumed mass begins to flow away.

4. CONCLUSION

In this work, we have shown that the outburst in the CN V1047 Cen (Nova Cen 2005), which appeared in 2019, is of the Z And-type – a type that has so far

been observed exclusively in the light curves of SySts (Sect. 3.1).

The 2019 outburst was powered by the accretion of the hydrogen-rich material on the surface of a steady-burning WD at rates of $\sim 2 \times 10^{-7} M_{\odot} \text{ yr}^{-1}$ that is above the upper limit of stable burning for a WD mass $\lesssim 0.7 M_{\odot}$. Following the theory, this led to the formation of a stellar wind blowing at rates $\gtrsim 10^{-6} M_{\odot} \text{ yr}^{-1}$ (Sects. 2.3 and 3.1). The wind was ionized by a $\sim 1.6 \times 10^5 \text{ K}$ hot and $\sim 5 \times 10^{37} \text{ erg s}^{-1}$ luminous, nuclear-burning WD giving rise to a large amount of nebular radiation ($EM \gtrsim 10^{60} \text{ cm}^{-3}$) that dominated the optical/NIR (Figs. 1 and 2, Tables 1 and 3). These characteristics are typical of Z And-type outbursts in SySts (see Sect. 1.1, and Sect. 3.5 for summary).

The presence of the Z And-type outburst in the CN binary indicates an extension of the nuclear burning time on the surface of the WD after the CN explosion. This may lead to a faster mass increase of the accreting WD, and thus to a faster evolution terminated by Type Ia supernova explosion. However, to better understand this possibility in the evolution of CVs, we need to know the nature of the donor star and how a nova explosion can affect it.

The authors thank the anonymous referee for constructive comments. This work was supported by a grant of the Slovak Academy of Sciences, VEGA No. 2/0003/25 and by the Slovak Research and Development Agency under the contract No. APVV-20-0148. We also acknowledge the variable-star observations from the AAVSO International Database contributed by observers worldwide and used in this research.

APPENDIX

A. MAGNITUDES OF THE TRUE CONTINUUM

Photometric magnitudes represent integrated fluxes that include both the continuum and the line spectrum. The presence of emission lines leads to brighter magnitudes than those of the continuum. The influence of an emission line on the measured magnitude, m_{obs} , is given by its equivalent width, the width of the photometric filter, and its transmission at the wavelength of the line. According to the method of Skopal (2007), we determined corrections $\Delta m = m_{\text{obs}} - m_{\text{cont}}$ for emission lines, where m_{cont} is the magnitude of the true continuum. Using the spectra of Aydi et al. (2022), we obtained corrections ΔB , ΔV , and ΔR_C (Table 2). The values of ΔB represent their lower limit since the spectra cover only part of the B filter. Similarly, corrections ΔI_C could be estimated only for days 74, 81 ($\Delta I_C \gtrsim -0.05$ mag), and 297, 303 ($\Delta I_C \approx -0.1$ mag, see Appendix D). In modeling the SED after the outburst, we assumed $\Delta I_C = -0.1$ mag. Magnitudes of the true continuum were used for the flux calibration of the optical spectra (Sect. 2.1) and for the color-diagram diagnostics (Sect. 2.4).

Table 2. Corrections of the B , V , and R_C magnitudes for emission lines measured on the spectra of Aydi et al. (2022).

Age ^a (days)	Spectrum range (nm)	ΔB (mag)	ΔV (mag)	ΔR_C (mag)
74	410–880	< -0.06 ^b	-0.07	-0.12
81	400–880	< -0.26	-0.08	-0.14
84	450–520	< -0.21 ^b	–	–
114	390–560	< -0.19 ^b	< -0.04	–
121	380–780	-0.26	-0.08	-0.23
130 ^b	450–890	–	-0.09	-0.22
143	380–780	-0.33	-0.08	-0.29
231	485–780	–	-0.09	-0.22
254	380–780	< -0.21 ^b	-0.12	-0.32
262	380–780	< -0.16 ^b	-0.13	-0.28
281	450–820	< -0.10 ^b	-0.12	-0.31
286	450–820	–	-0.08	-0.21
297	420–890	< -0.11 ^b	-0.13	-0.34
303	400–880	< -0.16 ^b	-0.10	-0.27
407	410–710	< -0.43	-0.40	-0.25

Notes.

^a As in Table 1.

^b Underexposed spectrum.

B. RELATIONSHIP BETWEEN L_{WD} AND EM

The enhanced mass outflow during outbursts converts more ionizing radiation from the WD into nebular emission than during quiescence (Sects. 1.1 and 2.3). In the limiting case, when all the ionizing photons are converted into the nebular emission, we can estimate the WD luminosity, L_{WD} , from the emission measure, EM , for the given WD temperature, T_{WD} , according to the expression (see Eq. (11) of Skopal et al. 2017),

$$L_{\text{WD}} = \alpha_{\text{B}}(\text{H}, T_e) EM \frac{\sigma T_{\text{WD}}^4}{f(T_{\text{WD}})}, \quad (\text{B1})$$

where $\alpha_{\text{B}}(\text{H}, T_e)$ is the total recombination coefficient to all but the ground state of hydrogen (i.e., describing a dense nebula, optically thick in the Lyman continuum; the so-called Case B). The corresponding radius, $R_{\text{WD}}^{\text{eff}}$, is determined

Table 3. Physical Parameters of the 2019 V1047 Cen Outburst Determined with the Aid of Emission Measure^a.

Age ^b (days)	T_{WD} (kK)	V^{d} (mag)	EM (10^{60} cm^{-3})	N_{rec} (10^{47} s^{-1})	L_{WD} ($10^{37} \text{ erg s}^{-1}$)	L_{H} (10^{47} s^{-1})	$R_{\text{WD}}^{\text{eff}}$ (R_{\odot})	\dot{M}_{WD} ($10^{-6} M_{\odot} \text{ yr}^{-1}$)
74	>200	15.58	1.27±0.11	1.27±0.11	>1.05	~6.41	~0.044	~0.7
81	>200	15.18	1.81±0.16	1.81±0.16	>1.50	~6.41	~0.052	~0.9
84	175±10	15.06	2.04±0.18	2.04±0.18	1.52±0.37	7.12 ^{+1.44} _{-1.07}	0.07±0.01	1.12±0.15
86	175±10	15.20	1.40±0.10 ^c	1.40±0.10	1.04±0.12	7.39 ^{+1.46} _{-1.34}	0.06±0.01	0.85±0.12
114	173±10	14.94	2.35±0.21	2.35±0.21	1.73±0.42	7.18 ^{+1.46} _{-1.34}	0.08±0.01	1.26±0.18
118	176±10	14.92	3.30±0.20 ^c	3.30±0.20	2.46±0.26	7.29 ^{+1.59} _{-1.46}	0.09±0.01	1.70±0.17
121	178±10	15.00	2.14±0.19	2.14±0.19	1.61±0.39	7.03 ^{+1.42} _{-1.31}	0.07±0.01	1.14±0.17
130	173±10	14.66	2.90±0.26	2.90±0.26	2.14±0.54	7.18 ^{+1.46} _{-1.34}	0.08±0.01	1.50±0.23
143	185±10	15.32	1.59±0.14	1.59±0.14	1.24±0.30	6.82 ^{+1.37} _{-1.27}	0.06±0.01	0.86±0.15
254	151±10	14.57	2.62±0.24	2.62±0.24	1.75±0.44	7.93 ^{+1.63} _{-1.50}	0.10±0.02	1.57±0.24
262	146±10	14.37	3.12±0.28	3.12±0.28	2.04±0.51	8.11 ^{+1.67} _{-1.53}	0.11±0.02	1.85±0.29
281	118±10	13.82	5.23±0.47	8.00±0.72	4.59±1.29	9.24 ^{+1.88} _{-1.75}	0.26±0.06	3.77±0.61
303	136±10	13.83	5.28±0.47	8.08±0.72	5.04±1.44	8.50 ^{+1.75} _{-1.28}	0.21±0.04	3.34±0.53
308	136±10	14.20	4.90±0.30 ^c	7.50±0.46	4.37±0.47	7.87 ^{+1.89} _{-1.74}	0.19±0.02	3.07±0.35

Notes.

^a Designation as in Sections 2.2, 2.3, and Appendix B. EM from V according to Eq. (2) or Table 1^c; L_{WD} from T_{WD} and EM according to Eq. (B1); $R_{\text{WD}}^{\text{eff}}$ from the Stefan-Boltzmann law; \dot{M}_{WD} from Eq. (3); N_{rec} from Eq. (B4), and L_{H} from Eq. (B3). T_{WD} was determined from optical spectra available at given dates (Sect. 2.2).

^b As in Table 1,

^c EM from SED models (Table 1),

^d Observed V magnitude from Fig. 2 a.

by the Stefan-Boltzmann law. The function $f(T_{\text{WD}})$ determines the flux of ionizing photons emitted by 1 cm^2 area of the blackbody source ($\text{cm}^{-2} \text{ s}^{-1}$) and can be expressed as

$$f(T_{\text{WD}}) = \frac{\pi}{hc} \int_0^{912\text{\AA}} \lambda B_{\lambda}(T_{\text{WD}}) d\lambda. \quad (\text{B2})$$

The total flux of hydrogen ionizing photons, L_{H} (s^{-1}), emitted by the WD pseudophotosphere is (see Eq. (11) of Skopal 2001)

$$L_{\text{H}} = \frac{L_{\text{WD}}}{\sigma T_{\text{WD}}^4} f(T_{\text{WD}}). \quad (\text{B3})$$

Assuming the hydrogen plasma, the coefficient $\alpha_{\text{B}}(\text{H}, T_e)$ expresses the ability of 1 electron and 1 proton in 1 cm^3 to recombine in 1 second ($\text{cm}^3 \text{ s}^{-1}$). Accordingly, physical meaning of the parameters EM (see Sect. 2.2) and $\alpha_{\text{B}}(\text{H}, T_e)$ determine the rate of recombinations within the nebule (i.e., the ionized wind), N_{rec} (s^{-1}), as

$$N_{\text{rec}} = \alpha_{\text{B}}(\text{H}, T_e) \times EM, \quad (\text{B4})$$

which is valid for the hydrogen plasma, heated by photoionizations.

In the case, when the outflowing particles are capable of converting only a part of the ionizing photons into the nebular emission, i.e., $L_{\text{H}} > N_{\text{rec}}$ (the so-called particle-bounded nebula), the value of L_{WD} according to Eq. (B1) is below its real value. Under this condition, increasing \dot{M}_{WD} increases N_{rec} , i.e., EM , and thus the brightness of the star, as the nebular continuum dominates the optical/NIR (Fig. 1, Eq. (2)). When $L_{\text{H}} = N_{\text{rec}}$ (the so-called ionization-bounded nebula), all the ionizing photons are absorbed within the nebula and converted to the nebular

emission producing a maximum EM . As a result, the value of L_{WD} from Eq. (B1) corresponds to the true value obtained from SED models (see Figs. 2 b and 4 during the maximum)⁵.

All physical parameters obtained with the aid of EM , estimated from (dereddened and emission-line-free) V magnitudes (Eq. (2)) and determined by SED models (Eq. (1)), as well as the corresponding auxiliary parameters N_{rec} (Eq. (B4)) and L_{H} (Eq. (B3)) are introduced in Table 3. In determining N_{rec} we used the coefficient $\alpha_{\text{B}}(\text{H}, 30,000 \text{ K}) = 1.0$ and $\alpha_{\text{B}}(\text{H}, 20,000 \text{ K}) = 1.53 \times 10^{-13} \text{ cm}^3 \text{ s}^{-1}$ for electron concentration 10^{10} cm^{-3} (Hummer & Storey 1987) during the first part of the 2019 outburst (day < 264) and during its maximum, respectively. In determining L_{H} we used L_{WD} obtained by SED modeling on days 86, 118, and 308 (Table 1), and their average value $(5.3 \pm 0.8) \times 10^{37} \text{ erg s}^{-1}$ for other days with available T_{WD} . The values of N_{rec} and L_{H} along the outburst are plotted in Fig. 4 and discussed in Sect. 3.3. Their uncertainties are described in Appendix C.

C. ESTIMATE OF UNCERTAINTIES

The uncertainty of the temperature T_{WD} is given by the accuracy of determining the He II $\lambda 4686/\text{H}\beta$ flux ratio, which depends on the S/N ratio and the blending of the He II line with the C III/N III emissions at 4640–4650 Å, eventually with the He I $\lambda 4713$ emission line. We estimated the S/N ratio at 5–10% and eliminated the blending by extracting the He II line using Gaussian functions. The advantage is that the line flux ratio reduces these errors. For higher T_{WD} , the method transfers a given error in the line ratio to a larger uncertainty in T_{WD} , and vice versa (see Fig. 5.1. of Gurzadyan 1997). However, smaller values of the line ratio, which correspond to a lower T_{WD} , are usually burdened by a larger error of the He II $\lambda 4686$ line flux. For spectra with a complicated continuum profile around He II $\lambda 4686$ and H β lines (days 74, 81, 130 and 407), instead of the flux ratio, we used the ratio of their equivalent widths, which is a source of additional errors. Taking all these limitations into account, we estimated errors in T_{WD} of less than 10%. Since their exact determination is difficult, we adopted an average uncertainty in T_{WD} of 10,000 K for all values.

To estimate the uncertainty of the angular radius, θ_{WD} , we scaled the Planck function for $T_{\text{WD}} \pm 10,000 \text{ K}$ to the mean values of NUV fluxes, because they fit well with the overall SED models. In this way, we obtained uncertainties of $\sim 4\%$ in θ_{WD} and thus also in $R_{\text{WD}}^{\text{eff}}$. Corresponding uncertainties in L_{WD} that include also those in T_{WD} are of 15–20% (see Table 1).

The uncertainty of the scaling factor, k_{N} and thus of the EM , is given by the accuracy of the optical/NIR continuum, which was estimated at $\sim 7\%$. The electron temperature T_{e} determines the slope of the nebular continuum. For the SED models, we estimated the maximum error in T_{e} to be about 15%.

To estimate uncertainties in the EM that was obtained from the V magnitude, we adopted the errors of the daily V -magnitude averages to 0.1 mag, which translates into uncertainties of $\sim 9\%$ in the EM (see Eq. (2)). Having uncertainties in EM and T_{WD} , we determined the uncertainty in L_{WD} as the root mean square error using the total differential of the function given by Eq. (B1). In this way, we obtained errors in L_{WD} between 24 and 28%. Similarly, we determined uncertainties for the effective radius $R_{\text{WD}}^{\text{eff}}$ given by the Stefan-Boltzman law for the errors in L_{WD} and T_{WD} . The errors of the parameters obtained indirectly using Eqs. (2) and (B1) are given in Table 3.

To estimate the uncertainties in \dot{M}_{WD} , we followed the theory of the optically thick wind in nova outbursts, according to which the matter is accelerated deep inside the pseudophotosphere (Kato & Hachisu 1994). Since the pseudophotosphere represents the optically thick/thin interface of the expanding wind, the wind cannot start there. However, the onset of the wind is not specified by theory, nor can it be determined from observations. Therefore, we adopted the average value from both limiting cases as a reasonable estimate of \dot{M}_{WD} (see Sect. 2.3), whose maximum error includes the uncertainty of EM and $R_{\text{WD}}^{\text{eff}}$. This gives uncertainties in \dot{M}_{WD} of around 8% in Table 1 and 13 to 17% in Table 3.

For L_{H} (Eq. (B3)), we determined the maximum error that correspond to the uncertainties in L_{WD} and the different values of the $f(T_{\text{WD}})$ function for the lower and upper limits of a given T_{WD} . The error values are in the range of 15 to 20%. Since the $f(T_{\text{WD}})$ function decreases unevenly with T_{WD} (for $T_{\text{WD}} > 73,000 \text{ K}$), we determined the lower and upper error limits in L_{H} separately. Finally, the uncertainties in N_{rec} reflect those in EM (see Eq. (B4)).

D. RECONSTRUCTION OF COLOR DIAGRAMS

Using data from the AAVSO database from day 77 to day 407, we determined the $B - V$ and $V - I_{\text{C}}$ indices from the average values of B , V , and I_{C} magnitudes observed within 1 day. In this way, we obtained the color indices

⁵ Possible brightness increase due to the stellar radiation from the hot WD is very small in the optical/NIR, but can be more pronounced in the far-UV

measured in 238 days along the 2019 outburst of V1047 Cen. We dereddened the magnitudes with $E_{B-V} = 1.0$ mag using the extinction curve of Cardelli et al. (1989) that increased the brightness in B , V , and I_C by 4.106, 3.096, and 1.897 mag, respectively.

To obtain the magnitudes of the true continuum, we corrected them for the effect of emission lines (see Appendix A). For the B magnitude we adopted $\Delta B = -0.3$ mag determined from well-exposed spectra on days 121 and 143 that cover the whole passband. For V we used $\Delta V = -0.05$ and -0.1 mag during the plateau phase and the maximum, respectively (green and red points in Fig. 3; Table 2). In the case of I_C magnitudes, we estimated ΔI_C to -0.1 mag during the maximum (day 297 and 303), when strong $O\text{I}\lambda 8446$ and $\lambda 7772$ appeared in the spectrum, while $\Delta I_C \gtrsim -0.05$ was estimated for days 74 and 81, when these lines were absent. Moreover, according to SED models, we subtracted the contribution from the WD in the B band that corresponds to ≈ 0.2 mag (it is negligible in other photometric bands). Adding these corrections to the reddening-free B , V , and I_C magnitudes, we estimated color indices of the true continuum as $(B + 0.3 + 0.2) - (V + 0.1) = B - V + 0.4$ and $(V + 0.05/0.1) - (I_C + 0.05/0.1) = V - I_C$.

Finally, we determined the theoretical color indices of the hydrogen nebular continuum by calculating the volume emission coefficient $\varepsilon_\lambda(\text{H}, T_e)$ (see Eq. (1)) at the effective wavelengths of the photometric B , V , and I_C passbands as a function of T_e and converted the corresponding fluxes to magnitudes according to the calibration of Henden & Kaitchuck (1982) and Bessell (1979).

A comparison of the color indices of the true continuum derived from the observations and the theoretical indices is shown in Figure 3. The large scatter in the measured values ($\gtrsim 0.1$ mag) is mainly due to systematic errors caused by the different instrumental systems used by different observers and their treatment of the raw data. Another source of uncertainty is the variability of the equivalent widths of the emission lines along the outburst due to variations in both the continuum and the lines.

REFERENCES

- Allen, D. A. 1980, MNRAS, 192, 521, doi: [10.1093/mnras/192.3.521](https://doi.org/10.1093/mnras/192.3.521)
- Aydi, E., Buckley, H. D. A., Mroz, P., et al. 2019a, The Astronomer’s Telegram, 12885, 1
- Aydi, E., Strader, J., Chomiuk, L., et al. 2019b, The Astronomer’s Telegram, 12975, 1
- Aydi, E., Sokolovsky, K. V., Bright, J. S., et al. 2022, ApJ, 939, 6, doi: [10.3847/1538-4357/ac913b](https://doi.org/10.3847/1538-4357/ac913b)
- Balman, Ş. 2020, Advances in Space Research, 66, 1097, doi: [10.1016/j.asr.2020.05.031](https://doi.org/10.1016/j.asr.2020.05.031)
- Belloni, D., & Schreiber, M. R. 2023, in Handbook of X-ray and Gamma-ray Astrophysics, 129, doi: [10.1007/978-981-16-4544-0_98-1](https://doi.org/10.1007/978-981-16-4544-0_98-1)
- Belyakina, T. S. 1991, Bulletin Crimean Astrophysical Observatory, 83, 104
- Bessell, M. S. 1979, PASP, 91, 589, doi: [10.1086/130542](https://doi.org/10.1086/130542)
- Bode, M. F., & Evans, A. 2008, Classical Novae, Vol. 43, doi: [10.1017/CBO9780511536168](https://doi.org/10.1017/CBO9780511536168)
- Cannizzo, J. K., Smale, A. P., Wood, M. A., Still, M. D., & Howell, S. B. 2012, ApJ, 747, 117, doi: [10.1088/0004-637X/747/2/117](https://doi.org/10.1088/0004-637X/747/2/117)
- Cardelli, J. A., Clayton, G. C., & Mathis, J. S. 1989, ApJ, 345, 245, doi: [10.1086/167900](https://doi.org/10.1086/167900)
- Chochol, D., Hric, L., Urban, Z., et al. 1993, A&A, 277, 103
- Cúneo, V. A., Kenyon, S. J., Gómez, M. N., et al. 2018, MNRAS, 479, 2728, doi: [10.1093/mnras/sty1686](https://doi.org/10.1093/mnras/sty1686)
- Delgado, A., Harrison, D., Hodgkin, S., et al. 2019, Transient Name Server Discovery Report, 2019-985, 1
- Di Mille, F., Congiu, E., Morrell, N., & Boutsia, K. 2019, The Astronomer’s Telegram, 12893, 1
- Fernandez-Castro, T., Gonzalez-Riestra, R., Cassatella, A., Taylor, A. R., & Seaquist, E. R. 1995, ApJ, 442, 366, doi: [10.1086/175446](https://doi.org/10.1086/175446)
- Fujimoto, M. Y. 1982a, ApJ, 257, 752, doi: [10.1086/160029](https://doi.org/10.1086/160029)
- . 1982b, ApJ, 257, 767, doi: [10.1086/160030](https://doi.org/10.1086/160030)
- Gallagher, J. S., & Starrfield, S. 1978, ARA&A, 16, 171, doi: [10.1146/annurev.aa.16.090178.001131](https://doi.org/10.1146/annurev.aa.16.090178.001131)
- Geballe, T. R., Banerjee, D. P. K., Evans, A., et al. 2019a, The Astronomer’s Telegram, 12923, 1
- . 2019b, ApJL, 886, L14, doi: [10.3847/2041-8213/ab5310](https://doi.org/10.3847/2041-8213/ab5310)
- Ginzburg, S., & Quataert, E. 2021, MNRAS, 507, 475, doi: [10.1093/mnras/stab2170](https://doi.org/10.1093/mnras/stab2170)
- González-Riestra, R., Viotti, R. F., Iijima, T., et al. 2008, A&A, 481, 725, doi: [10.1051/0004-6361:20078593](https://doi.org/10.1051/0004-6361:20078593)
- Greiner, J. 1996a, Supersoft X-Ray Sources, Vol. 472, doi: [10.1007/BFb0102238](https://doi.org/10.1007/BFb0102238)
- . 1996b, in Supersoft X-Ray Sources, ed. J. Greiner, Vol. 472, 299, doi: [10.1007/BFb0102274](https://doi.org/10.1007/BFb0102274)
- Gurzadyan, G. A. 1997, The Physics and Dynamics of Planetary Nebulae
- Hachisu, I., Kato, M., & Nomoto, K. 1996, ApJL, 470, L97, doi: [10.1086/310303](https://doi.org/10.1086/310303)

- Henden, A. A., & Kaitchuck, R. H. 1982, *Astronomical photometry*
- Hillman, Y., Shara, M. M., Prialnik, D., & Kovetz, A. 2020, *Nature Astronomy*, 4, 886, doi: [10.1038/s41550-020-1062-y](https://doi.org/10.1038/s41550-020-1062-y)
- Hummer, D. G., & Storey, P. J. 1987, *MNRAS*, 224, 801, doi: [10.1093/mnras/224.3.801](https://doi.org/10.1093/mnras/224.3.801)
- Iijima, T. 1981, in *NATO Advanced Study Institute (ASI) Series C, Vol. 69, Photometric and Spectroscopic Binary Systems*, 517, doi: [10.1007/978-94-009-8486-8_27](https://doi.org/10.1007/978-94-009-8486-8_27)
- Kato, M., & Hachisu, I. 1994, *Astrophys. J.*, 437, 802, doi: [10.1086/175041](https://doi.org/10.1086/175041)
- Kato, M., Mikolajewska, J., & Hachisu, I. 2012, *ApJ*, 750, 5, doi: [10.1088/0004-637X/750/1/5](https://doi.org/10.1088/0004-637X/750/1/5)
- Kenyon, S. J. 1986, *The symbiotic stars* (Cambridge: Cambridge University Press)
- Kenyon, S. J., Mikolajewska, J., Mikolajewski, M., Polidan, R. S., & Slovak, M. H. 1993, *AJ*, 106, 1573, doi: [10.1086/116749](https://doi.org/10.1086/116749)
- Kenyon, S. J., & Truran, J. W. 1983, *ApJ*, 273, 280, doi: [10.1086/161367](https://doi.org/10.1086/161367)
- Kovetz, A., Prialnik, D., & Shara, M. M. 1988, *Astrophys. J.*, 325, 828, doi: [10.1086/166053](https://doi.org/10.1086/166053)
- Lamers, H. J. G. L. M., & Cassinelli, J. P. 1999, *Introduction to Stellar Winds*
- Lasota, J.-P. 2001, *NewAR*, 45, 449, doi: [10.1016/S1387-6473\(01\)00112-9](https://doi.org/10.1016/S1387-6473(01)00112-9)
- Leibowitz, E. M., & Formigini, L. 2008, *MNRAS*, 385, 445, doi: [10.1111/j.1365-2966.2008.12847.x](https://doi.org/10.1111/j.1365-2966.2008.12847.x)
- Liller, W., Aguiar, J. G. D. S., & Amorim, A. 2005, *Central Bureau Electronic Telegrams*, 215, 1
- Mauche, C. W. 2004, *ApJ*, 610, 422, doi: [10.1086/421438](https://doi.org/10.1086/421438)
- McKeever, J., Lutz, J., Wallerstein, G., Munari, U., & Siviero, A. 2011, *PASP*, 123, 1062, doi: [10.1086/662076](https://doi.org/10.1086/662076)
- Mohamed, S., & Podsiadlowski, P. 2012, *Baltic Astronomy*, 21, 88, doi: [10.1515/astro-2017-0362](https://doi.org/10.1515/astro-2017-0362)
- Mroz, P., & Udalski, A. 2019, *The Astronomer's Telegram*, 12876, 1
- Muerset, U., Nussbaumer, H., Schmid, H. M., & Vogel, M. 1991, *A&A*, 248, 458
- Mukai, K. 2017, *PASP*, 129, 062001, doi: [10.1088/1538-3873/aa6736](https://doi.org/10.1088/1538-3873/aa6736)
- Munari, U. 2024, *arXiv e-prints*, arXiv:2412.20499, doi: [10.48550/arXiv.2412.20499](https://doi.org/10.48550/arXiv.2412.20499)
- Muerset, U., & Nussbaumer, H. 1994, *A&A*, 282, 586
- Ness, J. U., Schwarz, G., Starrfield, S., et al. 2008, *Astron. J.*, 135, 1328, doi: [10.1088/0004-6256/135/4/1328](https://doi.org/10.1088/0004-6256/135/4/1328)
- Nomoto, K. 1982, *ApJ*, 253, 798, doi: [10.1086/159682](https://doi.org/10.1086/159682)
- Nomoto, K., Saio, H., Kato, M., & Hachisu, I. 2007, *ApJ*, 663, 1269, doi: [10.1086/518465](https://doi.org/10.1086/518465)
- Oegelman, H., Orio, M., Krautter, J., & Starrfield, S. 1993, *Nature*, 361, 331, doi: [10.1038/361331a0](https://doi.org/10.1038/361331a0)
- Osaki, Y. 1974, *PASJ*, 26, 429
- Paczynski, B., & Rudak, B. 1980, *A&A*, 82, 349
- Paczynski, B., & Zytkow, A. N. 1978, *ApJ*, 222, 604, doi: [10.1086/156176](https://doi.org/10.1086/156176)
- Poole, T. S., Breeveld, A. A., Page, M. J., et al. 2008, *MNRAS*, 383, 627, doi: [10.1111/j.1365-2966.2007.12563.x](https://doi.org/10.1111/j.1365-2966.2007.12563.x)
- Prialnik, D., & Kovetz, A. 1995, *ApJ*, 445, 789, doi: [10.1086/175741](https://doi.org/10.1086/175741)
- Saeedi, S., Sasaki, M., & Ducci, L. 2018, *Mon. Not. R. Astron. Soc.*, 473, 440, doi: [10.1093/mnras/stx2354](https://doi.org/10.1093/mnras/stx2354)
- Seaquist, E. R., & Taylor, A. R. 1992, *ApJ*, 387, 624, doi: [10.1086/171112](https://doi.org/10.1086/171112)
- Sekeráš, M., Skopal, A., Shugarov, S., et al. 2019, *Contributions of the Astronomical Observatory Skalnaté Pleso*, 49, 19, doi: [10.48550/arXiv.1904.05555](https://doi.org/10.48550/arXiv.1904.05555)
- Shagatova, N., Skopal, A., & Cariková, Z. 2016, *A&A*, 588, A83, doi: [10.1051/0004-6361/201525645](https://doi.org/10.1051/0004-6361/201525645)
- Shara, M. M. 1989, *PASP*, 101, 5, doi: [10.1086/132400](https://doi.org/10.1086/132400)
- Shen, K. J., & Bildsten, L. 2007, *ApJ*, 660, 1444, doi: [10.1086/513457](https://doi.org/10.1086/513457)
- Sienkiewicz, R. 1980, *A&A*, 85, 295
- Sion, E. M. 2023, *Accreting White Dwarfs: From exoplanetary probes to classical novae and Type Ia supernovae*, doi: [10.1088/2514-3433/ac930c](https://doi.org/10.1088/2514-3433/ac930c)
- Skopal, A. 2001, *A&A*, 366, 157, doi: [10.1051/0004-6361:20000217](https://doi.org/10.1051/0004-6361:20000217)
- . 2005, *A&A*, 440, 995, doi: [10.1051/0004-6361:20034262](https://doi.org/10.1051/0004-6361:20034262)
- . 2006, *A&A*, 457, 1003, doi: [10.1051/0004-6361:20064935](https://doi.org/10.1051/0004-6361:20064935)
- . 2007, *NewA*, 12, 597, doi: [10.1016/j.newast.2007.04.003](https://doi.org/10.1016/j.newast.2007.04.003)
- . 2008, *Journal of the American Association of Variable Star Observers (JAAVSO)*, 36, 9, <https://arxiv.org/abs/0805.1222>
- . 2015, *New Astron.*, 36, 116, doi: [10.1016/j.newast.2013.10.009](https://doi.org/10.1016/j.newast.2013.10.009)
- . 2022, *AJ*, 164, 145, doi: [10.3847/1538-3881/ac897d](https://doi.org/10.3847/1538-3881/ac897d)
- Skopal, A., Tomov, N. A., & Tomova, M. T. 2013, *A&A*, 551, L10, doi: [10.1051/0004-6361/201321030](https://doi.org/10.1051/0004-6361/201321030)
- Skopal, A., Pribulla, T., Budaj, J., et al. 2009, *ApJ*, 690, 1222, doi: [10.1088/0004-637X/690/2/1222](https://doi.org/10.1088/0004-637X/690/2/1222)
- Skopal, A., Shugarov, S. Y., Sekeráš, M., et al. 2017, *A&A*, 604, A48, doi: [10.1051/0004-6361/201629593](https://doi.org/10.1051/0004-6361/201629593)
- Skopal, A., Shugarov, S. Y., Munari, U., et al. 2020, *A&A*, 636, A77, doi: [10.1051/0004-6361/201937199](https://doi.org/10.1051/0004-6361/201937199)
- Sokoloski, J., Lawrence, S., Crotts, A. P. S., & Mukai, K. 2016, in *Accretion Processes in Cosmic Sources*, 21, doi: [10.22323/1.288.0021](https://doi.org/10.22323/1.288.0021)
- Sonith, L. S., & Kamath, U. S. 2023, *MNRAS*, 526, 6381, doi: [10.1093/mnras/stad3121](https://doi.org/10.1093/mnras/stad3121)

- Starrfield, S., Iliadis, C., & Hix, W. R. 2016, *PASP*, 128, 051001, doi: [10.1088/1538-3873/128/963/051001](https://doi.org/10.1088/1538-3873/128/963/051001)
- Starrfield, S., Truran, J. W., Sparks, W. M., & Kutter, G. S. 1972, *ApJ*, 176, 169, doi: [10.1086/151619](https://doi.org/10.1086/151619)
- Tomov, T. V., Stoyanov, K. A., & Zamanov, R. K. 2016, *MNRAS*, 462, 4435, doi: [10.1093/mnras/stw2012](https://doi.org/10.1093/mnras/stw2012)
- Tutukov, A. V., & Yungelson, L. R. 1976, *Astrofizika*, 12, 521
- Udalski, A., Szymański, M. K., & Szymański, G. 2015, *AcA*, 65, 1, doi: [10.48550/arXiv.1504.05966](https://doi.org/10.48550/arXiv.1504.05966)
- van den Heuvel, E. P. J., Bhattacharya, D., Nomoto, K., & Rappaport, S. A. 1992, *Astron. Astrophys.*, 262, 97
- Walter, F. M., Battisti, A., Towers, S. E., Bond, H. E., & Stringfellow, G. S. 2012, *PASP*, 124, 1057, doi: [10.1086/668404](https://doi.org/10.1086/668404)
- Warner, B. 1995, *Cataclysmic variable stars*, Vol. 28 (Cambridge: Cambridge University Press)
- Wolf, W. M., Bildsten, L., Brooks, J., & Paxton, B. 2013, *ApJ*, 777, 136, doi: [10.1088/0004-637X/777/2/136](https://doi.org/10.1088/0004-637X/777/2/136)
- Yaron, O., Prialnik, D., Shara, M. M., & Kovetz, A. 2005, *ApJ*, 623, 398, doi: [10.1086/428435](https://doi.org/10.1086/428435)